

Resonance states in a cylindrical quantum dot with an external magnetic field

A Y Ramos and O Osenda

Facultad de Matemática, Astronomía y Física, Universidad Nacional de Córdoba,
Córdoba, Argentina and IFEG-CONICET, Ciudad Universitaria, X5016LAE
Córdoba, Argentina

Abstract. Bound and resonance states of quantum dots play a significant role in photo-absorption processes. In this work, we analyze a cylindrical quantum dot, its spectrum and, in particular, the behaviour of the lowest resonance state when a magnetic field is applied along the symmetry axis of the cylinder. To obtain the energy and width of the resonance we use the complex rotation method. As it is expected the structure of the spectrum is strongly influenced by the Landau levels associated to the magnetic field. We show how this structure affects the behaviour of the resonance state and that the binding of the resonance has a clear interpretation in terms of the Landau levels and the probability of localization of the resonance state. The localization probability and the fidelity of the lowest energy state allows to identify two different physical regimes, a large field-small quantum dot radius regime and a small field-large quantum dot radius, where the binding of the resonance is dominated by the field strength or the potential well, respectively.

PACS numbers: 73.22.-f, 31.15.-p

1. Introduction

The availability of quantum devices with characteristic length of only a few nanometer allows the implementation of a number of experimental setups that put under test the very foundations of Quantum Mechanics. The fact that the radius of a Landau level is of only a few nanometers for magnetic field strengths of around 10 Tesla allows the verification of the Aharonov-Bohm effect in quantum rings [1], which leads to the presence of persistent currents [2]. This persistent currents have been measured even for one electron states [3]. The quantum rings are formed by only one semiconductor material, and the fabrication of multiple concentric quantum rings (up to five) can be achieved with high quality and reliability [4].

On the other hand, one of the most studied nano-structures, the quantum dot, has been appointed as one of the most promising implementations of a single qubit [5, 6]. There has been a huge amount of work to circumvent the numerous associated problems: decoherence [7], the coupling between two qubits (to implement a two-qubit quantum gate) in double quantum dots has been studied extensively, in particular how it can be tuned using electric fields [8], magnetic fields [9], or the effect of the confinement of the double quantum dot in a quantum wire [10], etc.

When dealing with applied magnetic fields, most theoretical studies on quantum dots focus on strongly localized states, many times achieved using always-bounding potentials, as the three dimensional harmonic potential or impenetrable walls. The presence of a constant magnetic field, anyway, is equivalent to a two dimensional harmonic potential in the plane orthogonal to the field direction. Conversely, there are far less examples of studies considering finite potentials, in particular those whose shapes or features allow the presence of resonance states. There is a number of reason to study finite potentials, from charge transport situations to the effect of resonance states in luminescent quantum dots. The work by Bylicki and Jaskólski [11] analyzed the binding of shape resonances through the application of an external magnetic field. They considered an one-electron spherical quantum dot-quantum well structure (QDQW). In this work we consider a closely related problem with the purpose of a better understanding of the transition from a resonance state to a bounded one.

As has been said above, a constant magnetic field induces a two-dimensional harmonic potential that precludes the appearance of resonances in the plane orthogonal to the field, *i.e.* the loss of particles can take place **only** in the direction of the field, closing a number of decaying channels that would be available in absence of the field. In this sense, it renders almost irrelevant what particular shape has the binding potential, as long as it allows the appearance of resonances in the direction of the field. So, to avoid unnecessary complications, we consider a quantum dot model with cylindrical symmetry whose axis has the same direction that the magnetic field, besides we use the Effective Mass Approximation (EMA). As it is well known in this approximation the many-body interactions of the electron trapped in the quantum dot are reduced to a (simple) bounding potential, and all the parameters of the Hamiltonian, mass, dielectric

constants, and so on are taken as equal to the the bulk parameters.

Despite its apparent simplicity, the calculation of the resonance states of one electron trapped in a bounding potential with an external magnetic field is far from trivial, in particular for small enough strengths of the field since the Landau levels are bunched when the strength of the field goes to zero. To obtain the energy and width of the resonance states we employ the complex scaling method of Moiseyev [12] that, together with a variational \mathcal{L}^2 approximation for the wave function has been used to analyze the bound and resonance states of two electron quantum dots [13]. Moreover, as has been shown in [13], the fidelity of the variational eigenstates is a good tool to detect the resonance states. In this work we use the fidelity to study the binding of a resonance and show that it is signaled by a sharp change in the behavior of the fidelity. This feature is consistent with the behavior observed in the fidelity when the system experiments a quantum phase transition (in many-body models), is near the ionization threshold or to a resonance [13]. Recently, the application of concepts from Quantum Information Theory, as the fidelity or entanglement, has been very fruitful to analyze bound and resonance states in few body systems as two-electron quantum dots [13, 14, 15, 16], or two-electron He-like systems [17, 18].

The paper is organized as follows, in the quantum dot model and the variational approximation that provides approximate eigenvalues and eigenfunctions is presented Section 2, the analysis of the binding process is presented in Section 3, and finally we summarize and discuss our results in Section 4. Some rather lengthly and technical results, mostly matrix elements are deferred to the Appendices

2. Model

The bounding potential of the quantum dot is given by a piecewise function

$$V(\mathbf{r}) = \begin{cases} V_1, & \rho < a_\rho, \frac{a_z}{2} < |z_0| < \frac{a_z+b_z}{2} \\ -V_2, & \rho < a_\rho, |z| < \frac{a_z}{2} \\ 0, & \rho \geq a_\rho, |z| \geq \frac{a_z+b_z}{2} \end{cases} \quad (1)$$

i.e. the potential is a cylindrical well aligned with the z -axis, with two potential steps at the top and the bottom of the cylinder, where the radius of the cylinder is a_ρ , its height a_z , the depth of the potential well, $-V_2$, and the height of the potential steps, V_1 . This ensures that, for properly chosen constants a_z, b_z, a_ρ, V_1 and V_2 the one electron problem has resonance states without external field.

Even with the introduction of the external field the angular momentum L_z is a conserved quantity, and its eigenvalues good quantum numbers. So, we focus on states with zero angular momentum L_z . In this case, the Hamiltonian reads as

$$-\frac{1}{2\mu} \left(\frac{1}{\rho} \frac{\partial}{\partial \rho} \left(\rho \frac{\partial}{\partial \rho} \right) + \frac{\partial^2}{\partial z^2} \right) \Psi(\rho, z) + V(z, \rho) \Psi(\rho, z) = H_0 \Psi(\rho, z) = E \Psi(\rho, z) \quad (2)$$

where $V(\rho, z)$ is given by Equation 1, μ is the effective mass of the electron in the semiconductor material. The Equation is written in atomic units. If a magnetic field

$\mathbf{B} = B\hat{\mathbf{z}}$ is applied, there is a new term that must be incorporated to the LHS of Equation 2

$$H = H_0 + \frac{B^2}{8\mu}\rho^2, \quad (3)$$

The discrete spectrum and the resonance states of the model given by Eq. (3) can be obtained approximately using \mathcal{L}^2 variational functions [19], [20]. So, if Ψ_j are the exact eigenfunctions of the Hamiltonian, we look for variational approximations

$$\Psi_j \simeq \Psi_j^v = \sum_{i=1}^M c_i^{(j)} \Phi_i, \quad c_i^{(j)} = (\mathbf{c}^{(j)})_i; \quad j = 1, \dots, M. \quad (4)$$

where the Φ_i must be chosen adequately and M is the basis set size.

Since we are interested in null angular momentum eigenfunctions, and taking into account the symmetries of the Hamiltonian 3, we choose as basis functions

$$\Phi_i(\rho, z) = \psi_n(\eta\rho)\phi_t(\nu z), \quad (5)$$

where

$$\psi_n(\eta\rho) = \frac{1}{\sqrt{n+1}} \eta e^{-\eta\rho/2} \mathcal{L}_n^{(1)}(\eta\rho), \quad (6)$$

and

$$\phi_t(\nu z) = \sqrt{\frac{\nu}{2}} e^{-\nu|z|/2} \mathcal{L}_t^{(0)}(\nu|z|), \quad (7)$$

η and ν are the variational parameters. The matrix elements of the kinetic energy, the bounding potential and the magnetic field term are given in the Appendix. With all these matrix elements we get a variational eigenvalue problem

$$\tilde{\mathbf{H}}\mathbf{c}^{(j)} = E_j^v \mathbf{c}^{(j)}, \quad (8)$$

where the entries of the matrix $\tilde{\mathbf{H}}$ are given by

$$\tilde{\mathbf{H}}_{k,n,l,m} = \langle \psi_k \phi_n | H | \psi_l \phi_m \rangle \quad (9)$$

The ample range of materials and structures available to design self-assembled quantum dots precludes the possibility of a very general analysis, however, in part for comparison reasons, we use similar parameters than those used by Bylicki in [21] and Bilicky and Jaskólski in [11] to model a quantum dot quantum well structure made of gallium arsenide (GaAs) composites, *i.e.* $a_\rho = a_z = 7nm$, $b_z = 2.5nm$, $V_1 = 0.37eV$, $V_2 = 0.108844eV$, and $\mu = 0.041m_0$. The potential well depth is slightly different from the value used by Bylicky, but should be chosen so owed to the cylindrical symmetry employed in this work, conversely to the spherical one used by Bylicki. As we will show, this set of parameter is consistent with a resonance energy around $20meV$ with $B = 0$.

Figure 1 shows the variational eigenvalues obtained for $V_2 = 0.108844$, as functions of the magnetic field strength B . As can be appreciated, the eigenvalues are grouped in sets that are bounded between Landau levels given by $E_{LL}(M, n) = \frac{B}{\mu}(|M| + n + 1/2)$, where M is the azimuthal angular momentum (in our case $M = 0$), and $n = 0, 1, 2, \dots$

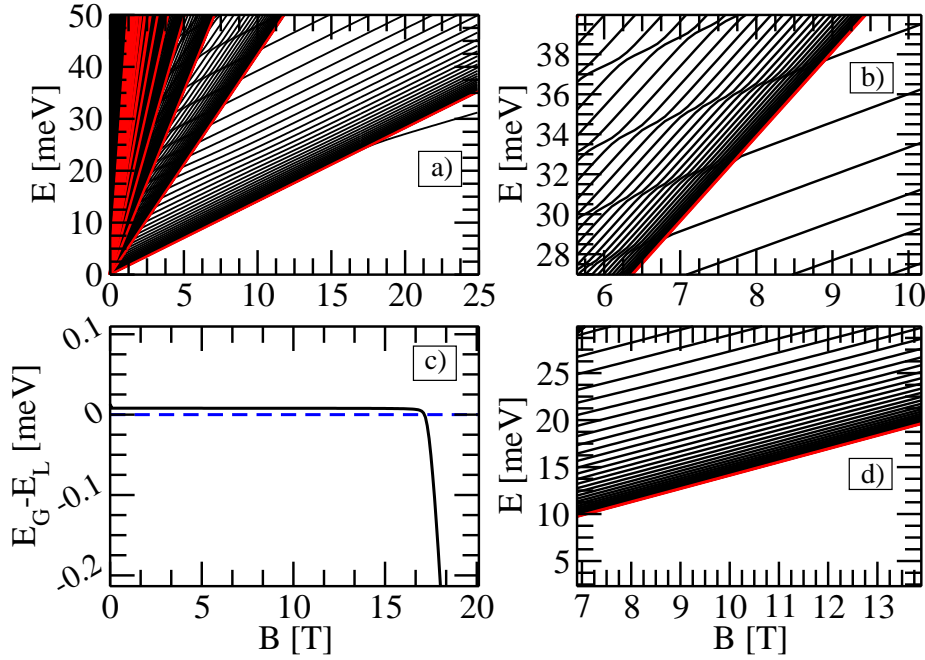


Figure 1. (Color on-line) The four panels show details of the variational spectrum and the Landau levels. a) The variational spectrum obtained with a basis set size $N = 2500$. Each black curve corresponds to a single eigenvalue and the red curves correspond to the exact Landau levels. b) This panel shows the limit between the zone limited by the two first Landau levels and the zone above the second Landau level. The only red curve corresponds to the second Landau level. The figure shows how the levels that collision with the second LL have several avoided crossings. c) The difference between the lowest variational eigenvalue and the first LL, when the lowest eigenvalue crosses below the first LL the eigenstate becomes localized. d) The eigenvalues above the first LL. The figure shows clearly how the eigenvalues are, basically, parallels to the LL and accumulate above it.

A pair of Landau levels delimits a region of the (B, E) plane, in this zone the eigenvalues are parallel to the lower Landau level, except for the appearance of avoided crossings.

As can be seen very clearly from Figure 1, the variational eigenvalues have the tendency to accumulate above the Landau levels. This feature is similar to the eigenvalue accumulation observed above the continuum threshold [13]. When a magnetic field is applied, each Landau level works as the bottom of a continuum leading to the eigenvalue accumulation observed in Figure 1. Another salient feature of the spectrum appears for large enough magnetic fields: one isolated eigenvalue with lower energy than the lowest Landau level. From physical point of view, the origin of this state can be understood as follows: for intermediate values of the magnetic fields the wave function of the electron looks like an harmonic oscillator wave function in the (ρ, ϕ) plane and as a free particle in the z direction. The spatial extent of the wave function on the plane is roughly equivalent to the radius of a Landau level, that is larger than the radius (in the plane) of the quantum dot. When the strength of the magnetic field is increased the radius of the lowest Landau level becomes smaller and smaller reaching, at some point, a size

similar to the radius of the quantum dot, at this point the state becomes localized. As we will show, the mechanism of localization can be quantified and strongly influences the behaviour of the resonance states whose energy lies near the localization point. The spectrum in Figure 1 was obtained using a basis set size $N = 2500$, all the other results shown in what follows were obtained using $N = 3200$.

3. Detecting the resonance states using complex exterior scaling

The calculation of the energy and width of resonance states offers a number of challenges that repeatedly leads to the formulation of new methods. Among the most widely used methods can be mentioned the complex scaling (or complex dilation) method [12], the complex absorbing potential method [22] and the density of states method [23]. Each one of these has its advantages and drawbacks. Because we are dealing with a piecewise potential we resort to the exterior complex scaling of Moiseyev [12]. This method is particularly appealing in our case since for $B \neq 0$, the complex scaling should be applied only to the z variable because this is the only direction available to the electron to get away from the bounding potential. The *exterior* of the method refers to the exterior of the region where the potential is not trivial so, for $B \neq 0$ the exterior complex scaling asks that

$$z \mapsto \begin{cases} z' & \text{if } |z| \leq \frac{a_z+b_z}{2}, \\ e^{i\theta} z' & \text{if } |z| \geq \frac{a+b}{2}, \end{cases} \quad (10)$$

where z is the coordinate to be complex scaled, and θ is the rotation angle. The complex scaling turns the non-normalizable scattering states of the continuum *and* the resonance states into normalizable states (with a different norm) which can be analyzed with the full variational approach usually employed in Hermitian problems.

Another advantage of the complex scaling method lies in the fact that its implementation depends on the availability of matrix elements that are similar to the ones calculated to obtain the entries of $\tilde{\mathbf{H}}_{k,n,l,m}$.

Figure 2 shows the behaviour of the energy and width of the lowest resonance as a function of the magnetic field strength. The binding of the resonance can be clearly observed, *i.e.* the width of the resonance drops to zero when the magnetic field strength increases its value. The exterior complex scaling methods works nicely for intermediate values of the magnetic field. Anyway, if $B \leq 5T$, or $B \geq 16T$, the convergence of the method is, at least, questionable. For small fields the method struggles to provide a reliable value for the resonance eigenvalue because, as can be appreciated from Figure 2, for $B \approx 5$ the resonance “enters” in the continuum above the second Landau level (Ll). In this region the approximate eigenvalues that enter from the region above the first Landau level “collide” with the eigenvalues that lie between the first and second LL. The successive collisions, and the corresponding avoided crossings, can be well appreciated in Figure 1b). In this sense the resonance disappears when there are not open channels to decay, bellow the first LL there is only a localized state, so there is no way for the resonance to avoid the binding.

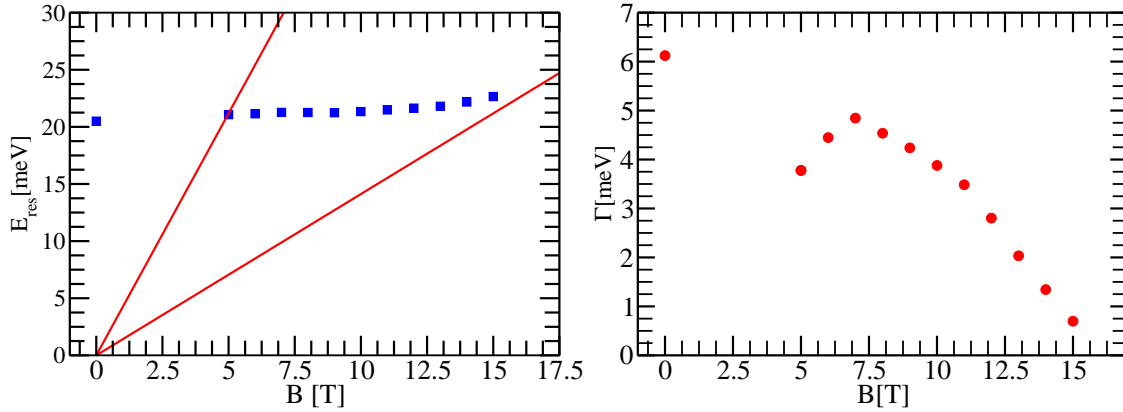


Figure 2. The real and imaginary parts of the resonance eigenvalue $E(\theta)$ vs the magnetic field strength. a) The solid square (blue) dots correspond to the energy of the resonance and the two solid lines correspond to the two lowest Landau level energies. The value for $B = 0$ was obtained performing the complex rotation in the coordinates ρ and z . b) The width of the resonance vs the magnetic field. As the magnetic field increases its value the width of the resonance goes to zero, signaling its binding.

The scenario between LL's can be better appreciated in Figure 3. The Figure shows the complex spectrum obtained when the complex rotation is performed accordingly with Equation 10 for different values of θ . In this Figure it is clear why the method is termed complex rotation, the continuum part of the spectrum now lies in the complex plane over straight lines, the angle between the lines and the real axis equal to 2θ . When $B \neq 0$, the data for different θ 's form “hand-fans” of data, *i.e.* sets of straight lines with a common origin in the real axis. Each one of these sets can be associated to a single LL, the leftmost hand-fan corresponds to first LL, the middle one to the second LL, and the rightmost to the third LL. Again, this structure can be attributed to role that each LL plays as the bottom of a continuum of levels. Effectively, the distance between the origins of each set of lines, over the real axis, is exactly equal to the distance between the LL at the magnetic field strength considered. As the magnetic field strength decreases, the data of the different fans overlaps making very difficult to distinguish the eigenvalues corresponding to the resonance.

Figure 3b) shows the trajectory in the complex plane of the eigenvalue associated to the resonance state. It is well known [12] that, to look for the best value obtainable from the method, the complex rotation must be performed for different values of θ and the best approximation corresponds to the stationary points of the trajectory. Actually, this is the recipe that we followed to obtain the data shown in Figure 2a) and b). It is possible to modify the method to obtain approximate resonance energies and widths for $B \leq 5T$, we will be back at this point latter on.

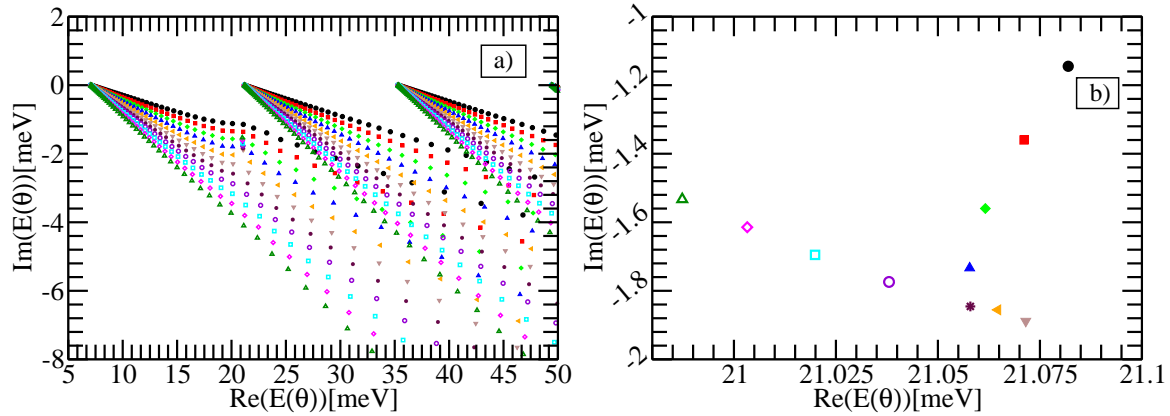


Figure 3. (Color on-line) a) The complex rotation eigenvalues *vs* the magnetic field. From top to bottom, the eigenvalues were obtained for $\theta = 0.1$ (black \bullet), $\theta = 0.11$ (red \blacksquare), $\theta = 0.12$ (green \blacklozenge), up to $\theta = 0.2$. The three fan-like sets of data are related to the first three LL's. It is clear that the leftmost fan and the central one start to overlap around 27 meV. For $B < 5T$ the overlap grows larger making more difficult to look for the resonance data. b) The θ trajectory of the resonance eigenvalue. The symbols correspond to the angles shown in panel a). These eigenvalues can be observed in panel a), they lie near the bump that presents the leftmost fan around 21 meV

3.1. Localization

The binding of the resonance for large enough magnetic field is a consequence of the strong localization experimented by the wave function. As a matter of fact, the localization is so sudden and clear that allows to follow the resonance through the spectrum. To quantify the localization of an approximate eigenfunction Ψ_j^v , we calculate the probability that the electron is localized in the potential well,

$$P_j = \int_{-\frac{a_z}{2}}^{\frac{a_z}{2}} \int_0^{a_\rho} |\Psi_j(\rho, z)|^2 d\rho dz, \quad (11)$$

where P_j is the probability attributable to the localization of Ψ_j^v .

Figure 4a) shows the probability P_1 as a function of the magnetic field strength for the lowest variational eigenvalue, while Figure 4b) shows the probability P_j for $j = 2, 3, \dots, 8$. The curves are shown in different panels because of their respective scale.

It is worth to mention that despite the variational eigenvalues near the localization do not show any sudden changes, except for the lowest one when it crosses the first LL, the probability of localization into the well is appreciable for a large number of eigenvalues. As we will shown later, the localization probability allows to follow the presence of the resonance from the localization threshold up to $B \sim 5T$.

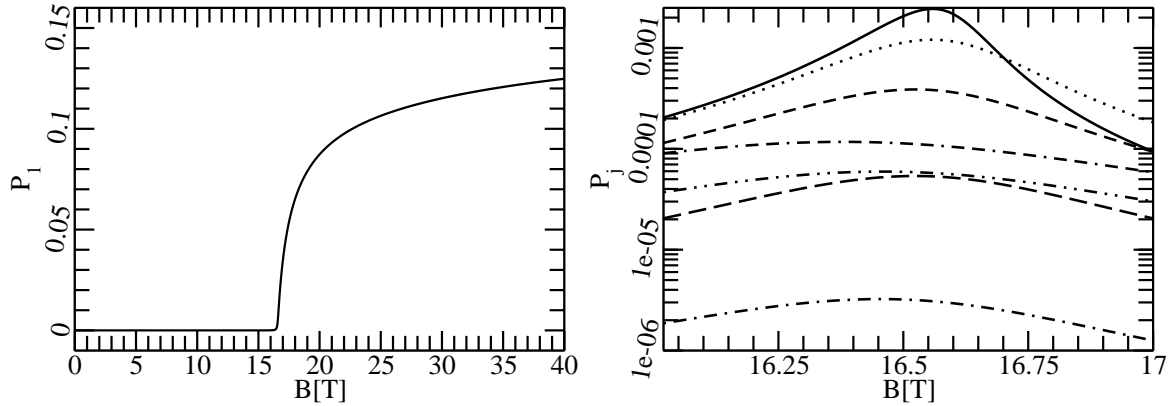


Figure 4. The localization probability *vs* the magnetic field strength. The left panel shows P_1 , *i.e.* the probability corresponding to the lowest variational eigenvalue. For small enough magnetic fields the variational eigenstate is extended over a region much larger than the characteristic lengths of the quantum dots. When $B \gtrsim 17T$ the eigenstate becomes localized, as shown by the sudden increase of P_1 . Once the lowest eigenstate becomes localized it remains so for even larger field strengths. **Right panel:** From top to bottom, P_2 (solid line), P_3 (dotted-line), ..., P_8 . The localization probabilities show a peak where the corresponding eigenvalue crosses near the resonance, after and before the eigenstate is extended.

3.2. Fidelity

For a given quantum state ψ , that depends on a parameter λ , a measure of how much it changes when the parameter is varied is given by the fidelity, \mathcal{F} , which is defined as

$$\mathcal{F}_{\Delta\lambda}(\lambda) = |\langle \psi(\lambda - \Delta\lambda), \psi(\lambda + \Delta\lambda) \rangle|^2, \quad (12)$$

where $\Delta\lambda$ is a small variation of the parameter. The fidelity has been extensively used to characterize the analytical properties of quantum states near a quantum phase transition in quantum spin chains models [24], quantum phases of matter [25], or bound and resonance states in atomic or quantum dot models [13]. In two-electron quantum dots, it has been shown that the fidelity of the approximate variational eigenstates detect the resonance states and allow to calculate approximately its energy [13]. To achieve this, the fidelity of many eigenstates should be calculated as a function of the external parameter that drives the system from bound to unbounded states. In this work, this parameter is the magnetic field strength.

From its definition, Equation 12, it is clear that most of the time $\mathcal{F}_{\Delta\lambda} \approx 1$, except for very special cases. On the other hand the fidelity should drop to zero if the system experiments a rather sudden change [24]. For this reason, often it is convenient to study the function

$$\mathcal{G}_n(\lambda) = 1 - |\langle \Psi_n^v(\lambda - \Delta\lambda), \Psi_n^v(\lambda + \Delta\lambda) \rangle|^2. \quad (13)$$

Figure 5 shows the behaviour of the \mathcal{G}_n function for $n = 1, 2, \dots, 6$, as function of the magnetic field strength. Each curve has a more or less well defined peak for a given value of the magnetic field, B_n . The values $E_n(B_n)$, *i.e.* the value of the

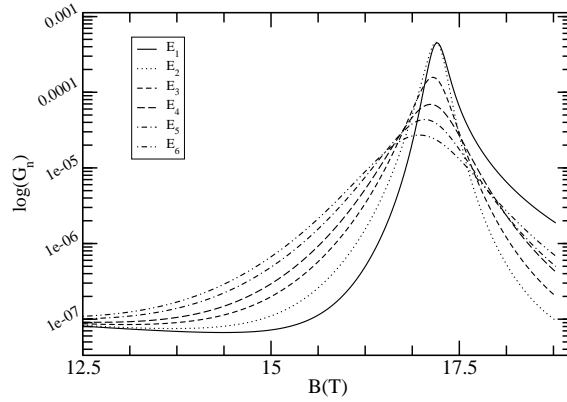


Figure 5. The function \mathcal{G}_n vs the magnetic field. The figure shows the function for the first six variational eigenvalues, $\mathcal{G}_1, \mathcal{G}_2, \dots, \mathcal{G}_6$, solid (—), dotted (·····), short-dashed (- - -), long-dashed (— — —), dot-dashed (— · —) and double dot-dashed (— · · —) lines respectively. The peak where each curve attains its maximum value is clearly appreciable. B_n is given by the abscissa of the peak (see the text).

variational eigenvalues at their respective peaks of the function \mathcal{G}_n , give a very good approximation for the resonance energy at the points B_n . As has been pointed out [13] this does not allow to obtain the resonance energy for every magnetic field strength value, nevertheless the method provides another tool to analyze resonance states. The fidelity method works best when the width of the resonance is not too wide, so it is to be expected that it will be more precise near the localization point.

Before presenting the results of the localization and fidelity methods with respect to the resonant states, we want to stress the relationship between both quantities. Let us call $B_p(a_\rho)$ the critical value of the magnetic field such that the localization probability of the first variational eigenvalue becomes noticeable for a given quantum dot radius a_ρ , and $B_F(a_\rho)$ the magnetic field value such that the function \mathcal{G}_1 attains its maximum value as a function of B . Figure 6 shows the values of both quantities, $B_p(a_\rho)$ and $B_F(a_\rho)$, for several values of the quantum dot radius a_ρ . The agreement between both critical quantities is striking.

At this point, we can summarize our results in Figure 7. The Figure shows the energy of the resonant state as a function of B , as it is obtained from the complex rotation, fidelity and localization methods.

From Figure 7 is rather clear that the localization methods is able to follow the resonance from the localization point until the second Landau level. The same can not be said about the fidelity results that, anyway, it is known that are valid for resonance with very small widths.

Above the second LL the complex rotation method should be complemented with some *ad hoc* assumptions to identify the points that belong to the θ -trajectory. The main assumption is rather physical: the complex rotated eigenvalues can be approximated by $E_{LL} + \tan 2\theta E_n$, *i.e.* they form a straight line in the complex plane that form an angle of 2θ with the x -axis, E_n is a variational eigenvalue. This approximation works nicely

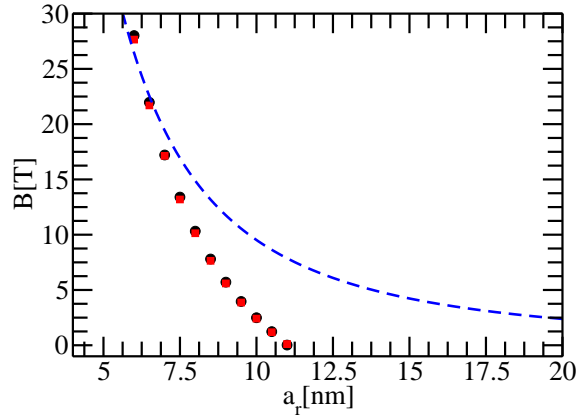


Figure 6. (Color on-line) The critical fields $B_p(a_\rho)$ and $B_F(a_\rho)$ vs the quantum dot radius. The localization probability critical field (red squared dots, \blacksquare) and the fidelity critical field (solid black dots, \bullet) data is shown for several quantum dot radius. The (blue) dashed curve correspond to the radius of the lowest LL as a function of the magnetic field. It is clear that for small quantum dot radius the localization takes place when the cylindrical wave function enters into the cylindrical QD. For larger QD's radius the localization is dominated by the quantum well potential and not by the magnetic field.

except near a resonance. The second assumption is similar: a given complex eigenvalue $E_\nu(\theta)$ should not change too much if θ is changed, say

$$|E_\nu(\theta + \delta\theta) - E_\nu(\theta)| \leq \delta\theta |E_\nu(\theta)|, \quad (14)$$

where $\delta\theta$ is small enough. Applying these assumptions and discarding complex eigenvalues that jump from a hand-fan to another (see Figure 3a)) it is feasible to obtain stabilized values for E_{res} above the second LL.

4. Discussion and Conclusions

The external magnetic field precludes the escape of the electron on the (ρ, ϕ) plane, for this reason the quantum dot bounding potential consists of a potential well and a potential step, to ensure the presence of resonance states. In this sense, the problem has several characteristic lengths, the quantum dot radius, the Landau levels radii, the length of the quantum dot along the z axis, and so on. The two lengths that come into play varying the magnetic field strength, for the set of parameters considered in this work, are the quantum dot radius and the lowest LL radius. The potential well depth and the other parameters of the QD were chosen to ensure that for $B = 0$ there were no bound states.

The localization probability is able to track down the resonance states from the localization point up to the second LL. Above the second LL the eigenvalues have too many avoided crossings, rendering the method useless. The many avoided crossings also prevent the use of the fidelity to detect the resonance above the second LL. The

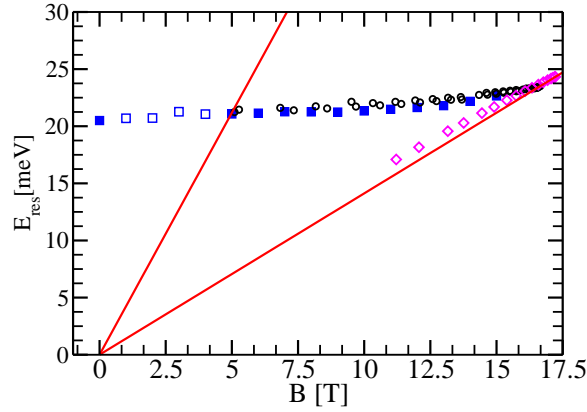


Figure 7. The resonance energy E_{res} calculated using the three methods depicted in the text, complex exterior scaling, localization probability, fidelity, the corresponding values are shown using blue square dots (■), black circles (○), and magenta diamonds (◇). The energy of the resonance in the region above the second LL can be obtained using a modified version of the complex rotation method and is shown using blue open squares dots (□).

large width of the resonance between the first and second LL seems to severely limit the ability of the fidelity to detect the resonance in this region. In two-electron dots the range of utility of the fidelity method could be related to the expectation value of the Coulomb repulsion between the electrons [13], right now we do not have a simple physical argument to explain the behaviour observed in this work.

Finally, both critical fields, $B_p(a_\rho)$ and $B_{\mathcal{F}}(a_\rho)$, show two clearly distinguishable regimes, for small quantum dot radius their values are given by the lowest Landau level radius, so both are proportional to $1/a_\rho^2$. For large enough quantum dot radius both critical fields show a different behaviour and, apparently, both are proportional to $(\alpha - \beta a_\rho)^2$, where α y β are constants. The extent of the small field regime can be tuned changing the parameters of the bounding potential 1, extending or reducing it. The critical behaviour of the eigenvalues in the transition region between the large field-small quantum dot radius and the small field-large quantum dot radius will be analyzed elsewhere.

Acknowledgments

We would like to acknowledge SECYT-UNC, CONICET, and MinCyT Córdoba for partial financial support of this project.

Appendix A. Some matrix elements

It is convenient to separate the kinetic energy matrix elements in two contributions, one corresponding to the radial coordinate,

$$\begin{aligned}
\langle \psi_n | T_\rho | \psi_s \rangle &= \left\langle \psi_n \left| -\frac{1}{2\mu} \nabla_r^2 \right| \psi_s \right\rangle \\
&= \frac{\eta}{\mu \sqrt{(n+1)(s+1)}} \left(\frac{1}{4} T_1 + \frac{1}{2} (T_2 + T_3) + T_4 \right)
\end{aligned} \tag{A.1}$$

and the other corresponding to the z coordinate,

$$\begin{aligned}
\langle \phi_t | T_z | \phi_r \rangle &= \left\langle \phi_t \left| -\frac{1}{2\mu} \nabla_z^2 \right| \phi_r \right\rangle \\
&= \frac{\eta}{2\mu \sqrt{(n+1)(s+1)}} \left(\frac{1}{4} T_{1z} + \frac{1}{2} (T_{2z} + T_{3z}) + T_{4z} \right)
\end{aligned} \tag{A.2}$$

where

$$\begin{aligned}
T_1 &= (n+1) \delta_{n,s}, \\
T_2 &= \sum_{p=0}^n \sum_{q=0}^{s-1} \frac{(-1)^{p+q} (n+1)! (s+1)! (p+q+1)!}{(n-1-p)! (2+p)! p! (s-q)! (1+q)! q!}, \\
T_3 &= \sum_{p=0}^{n-1} \sum_{q=0}^s \frac{(-1)^{p+q} (n+1)! (s+1)! (p+q+1)!}{(n-p)! (1+p)! p! (s-1-q)! (2+q)! q!}, \\
T_4 &= \sum_{p=0}^{n-1} \sum_{q=0}^{s-1} \frac{(-1)^{p+q} (n+1)! (s+1)! (p+q+1)!}{(n-1-p)! (2+p)! p! (s-1-q)! (2+q)! q!}
\end{aligned} \tag{A.3}$$

(A.4)

while

$$\begin{aligned}
T_{1z} &= \delta_{t,r}, \\
T_{2z} &= \sum_{d=0}^t \sum_{f=0}^{r-1} \frac{(-1)^{t+r} t! r! (d+f)!}{(t-d)! (d!)^2 (r-1-f)! (1+f)! f!},
\end{aligned} \tag{A.5}$$

$$\begin{aligned}
T_{3z} &= \sum_{d=0}^{t-1} \sum_{f=0}^r \frac{(-1)^{t+r} t! r! (d+f)!}{(t-1-d)! (1+d)! (r-f)! (f!)^2}, \\
T_{4z} &= \sum_{d=0}^{t-1} \sum_{f=0}^{r-1} \frac{(-1)^{t+r} t! r! (d+f)!}{(t-1-d)! (1+d)! d! (r-1-f)! (1+f)! f!}.
\end{aligned} \tag{A.6}$$

(A.7)

The matrix element of the bounding potential can be factorized owed to its piecewise character and using that there is a potential barrier on the z direction. We get that

$$\langle \psi_n \phi_t | V(\rho, z) | \psi_s \phi_r \rangle = -V_2 I_{V2} + V_1 I_{V1} \delta_{n,s}, \tag{A.8}$$

the barrier term is, obviously, proportional to V_1 , while the term proportional to V_2 corresponds to the matrix element of the potential well. The matrix elements I_{V2} and

I_{V1} are given by

$$I_{V2} = \frac{1}{\sqrt{(n+1)(s+1)}} \sum_{p=0}^n \sum_{q=0}^s \frac{(-1)^{p+q} (n+1)! (s+1)! I_{V21}}{(n-p)! (1+p)! p! (s-q)! (1+q)! q!} \\ \times \sum_{d=0}^t \sum_{f=0}^r \frac{(-1)^{d+f} t! r! I_{V22}}{(t-d)! (d!)^2 (r-f)! (f!)^2} \quad (\text{A.9})$$

$$I_{V1} = \frac{1}{\sqrt{(n+1)(s+1)}} \sum_{d=0}^t \sum_{f=0}^r \frac{(-1)^{d+r} t! r! I_{V11}}{(t-d)! (t!)^2 (r-f)! (f!)^2} \quad (\text{A.10})$$

and

$$I_{V21} = (p+q+1)! - e^{-\eta a} \sum_{k=0}^{p+q+1} \frac{(p+q+1)! (a\eta)^{p+q+1-k}}{(p+q+1-k)!}, \quad (\text{A.11})$$

$$I_{V22} = (d+f)! - e^{-\nu a/2} \sum_{g=0}^{d+f} \frac{(d+f)!}{(d+f-g)!} \left(\frac{\nu a}{2} \right)^{d+f-g}, \quad (\text{A.12})$$

$$I_{V11} = \sum_{k=0}^{d+f} \frac{(d+f)!}{(d+f-k)!} \\ \times \left(e^{-a\nu/2} \left(\frac{a\nu}{2} \right)^{d+f-k} - e^{-\frac{(a+b)\nu}{2}} \left(\frac{(a+b)\nu}{2} \right)^{d+f-k} \right). \quad (\text{A.13})$$

The matrix element of the magnetic field term reads as

$$\langle \psi_n | H_c | \psi_s \rangle = \frac{B^2}{8\mu\eta^2 \sqrt{(n+1)(s+1)}} \\ \times \sum_{p=0}^n \sum_{q=0}^s \frac{(-1)^{p+q} (n+1)! (s+1)! (p+q+3)!}{(n-p)! (1+p)! p! (s-q)! (1+q)! q!} \quad (\text{A.14})$$

- [1] Bayer M, Korkusinski M, Hawrylak P, Gutbrod T, Michel M, and Forchel A 2003 *Phys. Rev. Lett.* **90** 186801
- [2] Mailly D, Chapelier C and Benoit A 1993 *Phys. Rev. Lett.* **70** 2020
- [3] Kleemans N, Bominaar-Silkens I, Fomin V, Gladilin V, Granados D, Taboada A, García A, Offermans P, Zeitler U, Christianen P, Maan J, Devreese J and Koenraad P 2007 *Phys. Rev. Lett.* **99** 146808
- [4] Somaschini C, Bietti S, Koguchi N and Sanguinetti S 2009 *Nano Letters* **9** 3419
- [5] Loss D and DiVincenzo D 1998 *Phys. Rev. A* **57** 120
- [6] Takahashi R, Kono K, Tarucha S and Ono K 2011 *Phys. Rev. Lett.* **107** 026602
- [7] Petta R, Johnson A, Taylor J, Laird E, Yacoby A, Lukin M, Marcus C, Hanson M and Gossard A 2005 *Science* **309** 2180
- [8] Kwasniowski A and Adamowski J 2009 *J. Phys: Condens. Matter* **21** 235601
- [9] Szafran B, Peeters F and Bednarek S 2004 *Phys. Rev. B* **70** 125310
- [10] Zhang L, Melnikov D, Agarwal S and Leburton J 2008 *Phys. Rev. B* **78** 035418
- [11] Bylicki M and Jaskólski W 1999 *Phys. Rev. B* **60** 15924
- [12] Moiseyev N 1998 *Phys. Rep.* **302** 211
- [13] Pont F, Osenda O, Toloza J and Serra P 2010 *Phys. Rev. A* **81** 042518

- [14] Ferrón A, Osenda O and Serra P 2009 *Phys. Rev. A* **79** 032509
- [15] Nazmitdinov R, Simonović N, Plastino A and Chizhov A 2012 *J. Phys. A: Math. Theor.* **45** 205503
- [16] Abdullah S, Coe J and DAmico I 2009 *Phys. Rev. B* **80** 235302
- [17] Osenda O and Serra P 2007 *Phys. Rev. A* **75** 042331
- [18] Majtey A, Plastino A and Dehesa J 2012 *J. Phys. A: Math. Theor.* **45** 115309
- [19] Bylicki M, Jaskólski W, Stachów A and Diaz J 2005 *Phys. Rev. B* **72** 075434
- [20] A T Kruppa and K Arai, *Phys. Rev. A* **59**, 3556 (1999)
- [21] Bylicki M 2008 *J. Phys.: Conf. Ser.* **104** 012022
- [22] Sajeev Y, Vysotskiy V, Cederbaum L and Moiseyev N 2009 *J. Chem. Phys.* **131** 211102
- [23] Mandelshtam V A, Ravuri T R and Taylor H S 1993 *Phys. Rev. Lett.* **70** 1932
- [24] Zanardi P and Paunković N 2006 *Phys. Rev. E* **74** 031123
- [25] Garnerone S, Abasto D, Haas S and Zanardi P 2009 *Phys. Rev. A* **79** 032302